FEBS Letters 504 (2001) 166–172 FEBS 25154

Minireview

Two-dimensional crystals: a powerful approach to assess structure, function and dynamics of membrane proteins

Henning Stahlberg[a], Dimitrios Fotiadis[a], Simon Scheuring[a], Hervé Rémigy[a], Thomas Braun[a], Kaoru Mitsuoka[b], Yoshinori Fujiyoshi[b], Andreas Engel[a,*]

[a] *M.E. Müller-Institute for Structural Biology, Biozentrum, University of Basel, Klingelbergstr. 70, CH-4056 Basel, Switzerland*
[b] *Department of Biophysics, Faculty of Science, Kyoto University, Kitashirakawa, Sakyo-ku, Kyoto 606-8502, Japan*

Received 11 July 2001; accepted 23 July 2001

First published online 8 August 2001

Edited by Andreas Engel and Giorgio Semenza

Abstract Electron crystallography and atomic force microscopy allow the study of two-dimensional membrane protein crystals. While electron crystallography provides atomic scale three-dimensional density maps, atomic force microscopy gives insight into the surface structure and dynamics at sub-nanometer resolution. Importantly, the membrane protein studied is in its native environment and its function can be assessed directly. The approach allows both the atomic structure of the membrane protein and the dynamics of its surface to be analyzed. In this way, the function-related conformational changes can be assessed, thus providing a detailed insight on the molecular mechanisms of essential biological processes.

Key words: Two-dimensional crystallization; Electron crystallography; Atomic force microscopy

1. Introduction

Biological membranes define cell boundaries, delimit cellular compartments, and fulfill a wide spectrum of vital functions. These are provided by proteins embedded in the lipid bilayer. The wide range of membrane functions requires membrane proteins of diverse structures, all of which must meet the stringent prerequisite of a hydrophobic belt to warrant integration in the amphiphilic bilayer. Therefore, membrane proteins exhibit hydrophilic extrinsic and hydrophobic core surfaces. Consequently, solubilization and purification of integral membrane proteins necessitate the use of detergents.

Many membrane proteins are related to diseases such as cystic fibrosis, hyper- and hypotension, diabetes, and brain or lung edema, to mention only a few. In their major function as cell boundaries, membranes are involved not only in food, but also in drug uptake, and about 70% of all drug targets are membrane proteins.

Approximately 30% of the sequenced genes appear to encode membrane proteins. Sequence and function of many membrane proteins are now known, but by the end of 2000 only 37 structures were solved to atomic resolution, compared to more than 10 000 unique crystal structures of soluble proteins. Therefore, progress in membrane protein structure determination is mandatory for understanding biological membranes and their functions, an understanding that will also provide the basis for designing better therapeutics.

As result of the limited hydrophilic surfaces available for forming crystal contacts and the reduced stability, detergent-solubilized proteins do not readily form three-dimensional (3D) crystals suitable for X-ray analyses. Two methods have improved the success rate in 3D crystallization. First, the power of the immune system can be used to design precisely fitting hydrophilic extensions of a membrane protein. This method of producing F_v fragments for the 3D crystallization of membrane proteins is reviewed by Hunte (this issue, [41]). Second, 3D crystallization in cubic lipid phases that provide an environment which allows solubilized membrane proteins to diffuse and merge into micro crystals within the labyrinth of the cubic lipid system, has been successful for an increasing number of proteins (Nollert et al., this issue, [42]). A powerful alternative is the reconstitution into two-dimensional (2D) membrane protein crystals in the presence of lipids (Levy et al., this issue, [43]; [1]). This approach restores the native environment of membrane proteins as well as their biological activity [2]. Cryo-electron microscopy allows the 3D structure of the vitrified protein to be assessed at atomic resolution (Fig. 1). Complementary to this, the atomic force microscope (AFM) [3,4], depicts biological membranes in aqueous solutions and permits monitoring of the movement of single polypeptide loops. Thus, the combined application of these microscopy techniques will establish the 3D structure of different membrane proteins and will permit visualization of their conformational changes during catalytic cycles.

2. 2D crystallization

As with X-ray crystallography, production of 2D crystals is the major barrier in the structure determination by electron crystallography. Since membrane proteins are more stable when integrated in the bilayer, 2D crystallization offers some advantages compared to 3D crystallization, but solubilization, isolation and reconstitution protocols are as critical. Optimization of crystallization conditions is still empirical, because theories taking into account the properties of a mixture containing protein, lipid and detergent are too complex

*Corresponding author. Fax: (41)-61-267 2109.
E-mail address: andreas.engel@unibas.ch (A. Engel).

0014-5793/01/$20.00
PII: S0014-5793(01)02746-6

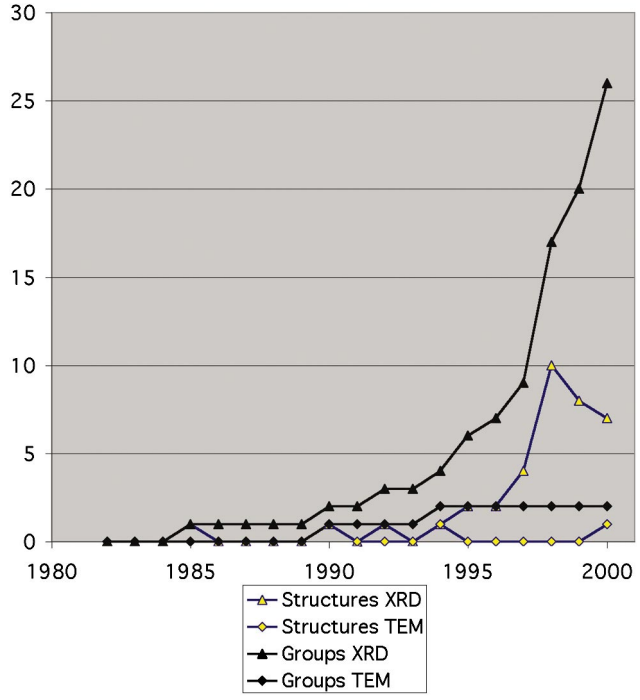

Fig. 1. Number of membrane protein structures submitted to the PDB per year up to 2000. Structures solved by X-ray crystallography (yellow triangles) are compared to structures solved by electron crystallography (yellow diamonds). The number of X-ray groups working on membrane proteins has sharply increased since 1995 (black triangles). In contrast, only the groups of R. Henderson [11] and Y. Fujiyoshi have submitted coordinates from electron analyses (black diamonds). The latter group has collaborated with W. Kühlbrandt (LHC2) [13] and A. Engel (AQP1) [14]. However, a significant number of membrane protein structures at a resolution of 5–8 Å have been presented by different electron microscopy groups. See also http://www.mpibp-frankfurt.mpg.de/michel/public/memprotstruct.html

for designing the reconstitution experiments. Such a mixture will assemble during detergent removal before the critical micelle concentration (cmc) of the detergent is reached. Four methods are currently used to achieve this condition: (i) dialysis of the detergent [5], (ii) its adsorption to Biobeads [6], (iii) dilution of the mixture to bring the detergent concentration towards the cmc [7], and (iv) the formation of monolayer crystals at the air–water interface by the lipid monolayer method (Levy et al., this issue, [43]). With a simple lipid–detergent mixture, the onset of assembly during detergent removal is manifested by a strong change of the particle size: lipids form long worm-like structures that ultimately convert to vesicles [8,9]. Similar drastic structural changes have been observed by light scattering during membrane–protein reconstitution [7], and control of this process appears to be essential for crystallization.

We have developed a temperature- and flow-controlled open dialysis device that is frequently used for 2D crystallization [5]. However, this method requires detergents with a cmc $>0.1\%$, which sometimes are not compatible with protein stability. Biobead-driven reconstitution is a simple and powerful approach, and is suitable for low-cmc detergents. Biobeads are also used for reconstitution of monolayer crystals at the air–water interface. Lactose permease crystallization became possible by producing pure protein at a concentration >3 mg/ml in 0.01% dodecyl maltoside three-fold dilution into lipids solubilized in decyl maltoside and subsequent dialysis-driven reconstitution [10] (Fig. 2). Based on this experience, approaches that include a pre-adsorption of excessive low-cmc detergents to Biobeads followed by dialysis will now be explored.

3. Electron crystallography

Recent results demonstrate that electron crystallography of 2D crystals has progressed to atomic resolution. A large number of proteins have been crystallized in 2D [1]. In several cases, the structures obtained by electron crystallography allowed significant atomic models to be built. These include bacteriorhodopsin (BR) [11,12], the light harvesting complex-2 (LH2) [13], aquaporin-1 (AQP1) [14,15], and tubulin [16]. However, many further membrane protein structures have been assessed by electron crystallography, and their structures evaluated to a resolution, which allowed the secondary structure to be clearly imaged [17–22]. Such knowledge combined with the information from sequence analysis frequently provides significant insight into the structure of the protein.

This progress is the result of an important improvement of the electron microscopes, first by the availability of field emission guns (FEG) operating at 200 or 300 kV, providing a highly coherent illumination of the sample, and second by the stable low-temperature stages developed in a pioneering effort by the Kyoto group [23]. To make electron crystallography a competitive method compared to X-ray crystallography, data acquisition must become a routine operation. Automated electron microscopy has made significant progress, and automated searches and data recording of crystalline samples appear to be technically feasible. While images of untilted samples kept at liquid nitrogen or liquid helium temperature have routinely given resolutions in a range of 3–4 Å, tilted samples often show a reduced resolution for diffraction spots that are far from the tilt axis. The reasons are (i) sample charging and (ii) crystal flatness. Spot-scan illumination appears to be one approach to reduce specimen charging effects [24]. Another possibility is sandwiching the frozen sample between two carbon films (Fujiyoshi et al., unpublished). Improvements in film flatness have been achieved by the use of special molybdenum grids [25,26]. In addition, smooth crystal curvatures should be compensated for by corresponding image processing approaches.

Several examples demonstrate that the achievable resolution is often close to or better than 3 Å (Fig. 3). The basis for this is clearly not the electron microscope alone, but also the crystalinity of the sample. Images are recorded mainly on film and subsequently digitized, but high resolution CCD cameras are likely to replace the film in the near future. A major advantage of CCD cameras is their high dynamic range (16 bit is achieved by all modern CCDs). This is now routinely exploited for recording electron diffraction patterns.

Combining image data from a large number of tilted images and merging them, if possible, with diffraction data from a similar data set allows the 3D Fourier transform of the membrane protein, and thus its 3D density map to be determined. The sophisticated image processing programs used to this end have been developed over many years by the groups of the Medical Research Council (MRC), Cambridge, London, UK [27]. They are currently used by most groups in the field,

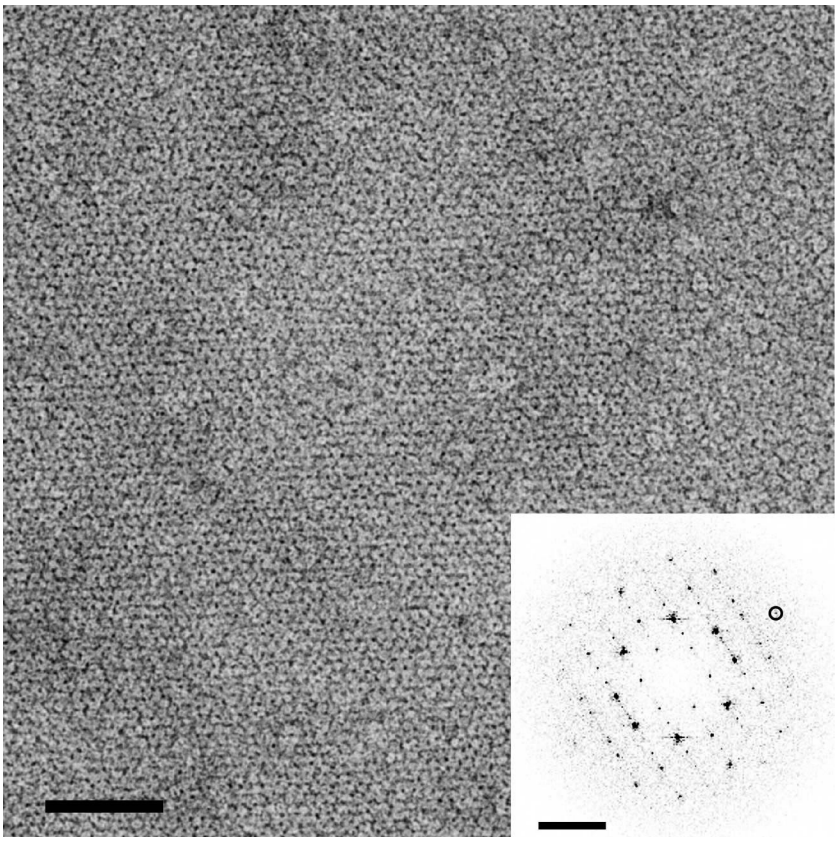

Fig. 2. Lactose permease resisted 3D crystallization since more than a decade. In contrast, 2D crystals have been produced from this flexible transporter by the dialysis method. Since the enzyme is difficult to keep in solution, crystallization experiments have not been reproducible, and the best data collected so far are from negatively stained samples. Scale bars: 50 nm (micrograph) and (50 Å)$^{-1}$ (diffraction pattern).

yielding 3D maps such as that shown in Fig. 4. Helices are seen clearly, exposing side chains of variable sizes in higher resolution maps. For refinement of the atomic models designed on the basis of such density maps, various packages commonly employed in X-ray crystallography have been used. A recent approach has taken advantage of a high-resolution structure of a homologous protein determined by X-ray analysis, the 2.2 Å structure of GlpF (the glycerol facilitator of *Escherichia coli*), to validate and refine the atomic structure of AQP1 determined by electron crystallography (de Groot et al., this issue, [44]).

It is instructive to compare data obtained by electron crys-

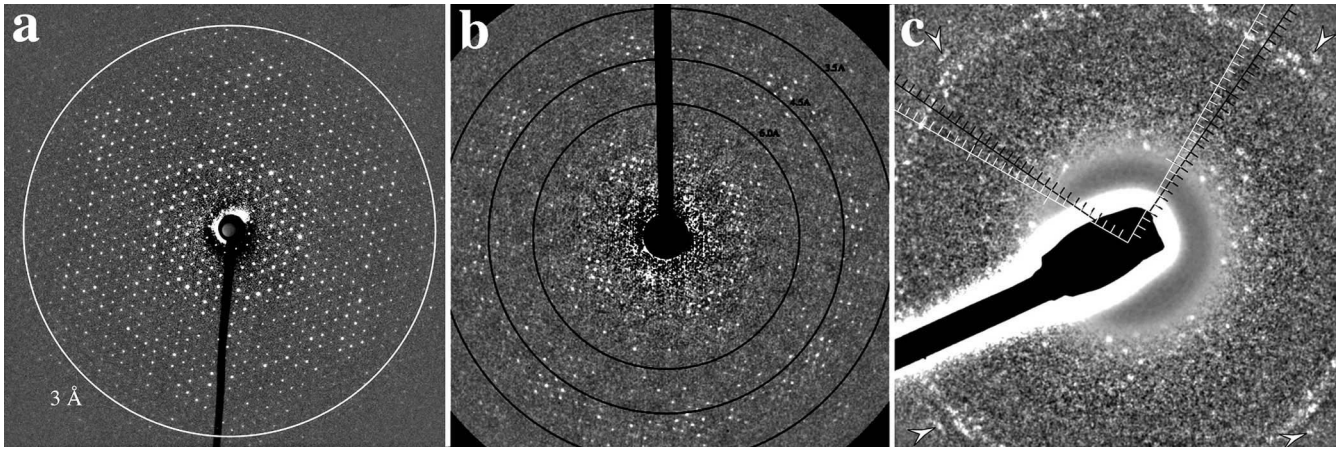

Fig. 3. Electron diffraction pattern demonstrate the order of 2D crystals. a: Purple membranes are highly ordered native 2D crystals of BR, the proton pump of *Halobacterium salinarium*. These trigonal lattices ($a = b = 62$ Å) can be merged to large sheets by detergent treatment. Prepared by the trehalose embedding method, these crystals diffract to better than 3 Å when recorded at liquid helium temperature. b: Tetragonal crystals reconstituted from AQP1 tetramers diffract to 3 Å. Since the unit cell is larger ($a = b = 96$ Å) than that of BR, the signal-to-noise ratio of the diffraction peaks is lower than in BR. c: GlpF assembles to highly ordered tetragonal lattices as well ($a = b = 104$ Å). The reflections at the periphery marked by arrows are at 3.6 Å. Diffraction pattern (a) and (b) were recorded with a 2×2 k CCD camera, whereas pattern (c) was taken with a 1×1 k CCD camera.

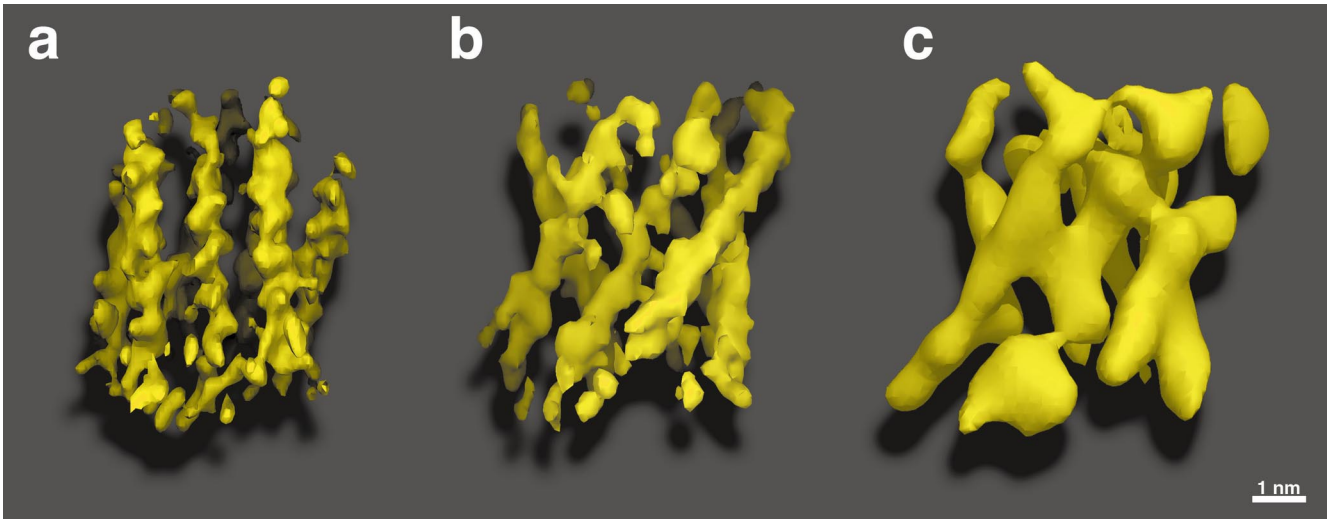

Fig. 4. Density maps calculated from electron diffraction patterns and electron micrographs recorded from trehalose embedded samples kept at liquid helium temperature. a: BR; b: AQP1; c: GlpF.

tallography with those from X-ray crystallography. Most recently, the atomic structures of AQP1 and GlpF have been compared (see de Groot et al., this issue, [44]). For BR, an evaluation has been presented by Luecke ([28]; Table 1). After alignment of the main chain atoms of the deposited BR structures with 1C3W (resolution 1.55 Å), using the program Swiss-PdbViewer, different BR atomic models have an overall root mean square deviation (RMS) compared to 1C3W ranging from 0.25 to 2.82 Å, whatever the structure determination method was used. Taking the best model obtained by electron crystallography (resolution 3 Å; [12]), the overall RMS is 1.49 Å. Significant variations emerge in the loops connecting the helices. A comparison of different BR structures with topographs acquired with the AFM revealed that the flexibility of loops monitored by AFM is reflected by the rather significant variations among different atomic models deposited in the PDB [29]. Loops exposed at the surface represent the sites of crystal contacts as well as the sites which interact with the support in case of 2D crystals adsorbed to a carbon film. Therefore, loops involved in crystal contacts are not necessarily in a native conformation, and the specific structures of loops in BR and also of rhodopsin found by X-ray crystallography may not represent the native state.

An interesting aspect of electron crystallography is the feasibility of rather fast data collection and processing. The 6.9 Å 3D map of GlpF has been determined from data recorded in 10 days on a 300 kV FEG instrument (Fig. 4c). Image processing took altogether 2 months, but can be accelerated significantly [30].

These examples not only show the power of electron crys-

Table 1
Overall comparison of deposited atomic BR structures with the highest resolution structure (1C3W, 1.55 Å resolution). By courtesy of H. Luecke [28]

PDB code	Main chain RMS (Å)	Side chain RMS (Å)	All atom RMS (Å)	Resolution (Å)	Method
1BRD	2.05	–	–	3.5	ED
2BRD	1.88	3.55	2.82	3.5	ED
1AT9	1.19	2.00	1.63	3.0	ED
2AT9	1.28	1.68	1.49	3.0	ED
1AP9[a]	2.11	3.46	–	2.35	X-ray, CLP
1AP9	1.68	3.28	2.58	2.35	X-ray, CLP
1QHJ[b]	0.46	1.14	0.86	1.9	X-ray, CLP
1QKO[c]	0.48	1.18	0.89	2.1	X-ray, CLP
1QKP[c]	0.48	1.17	0.89	2.1	X-ray, CLP
1CWQ[d]	1.21	2.01	1.64	2.3	X-ray, CLP
1CWQ[e]	1.34	2.19	1.81	2.3	X-ray, CLP
1BM1	0.89	2.15	1.63	3.5	X-ray, detergent
1BRR[f]	1.04	1.67	1.40	2.9	X-ray, detergent
1BRX	0.41	1.12	0.83	2.3	X-ray, CLP
1C8R	0.19	0.30	0.25	1.8	X-ray, CLP
1C8S[g]	0.55	0.98	0.79	2.0	X-ray, CLP

The main chain atoms of the deposited BR structures were aligned with 1C3W, using the program Swiss-PdbViewer. The RMS deviation between the aligned structures is given for main chain atoms only, side chain atoms only, and for all atoms.
[a]1AP9 as published in [39] and pre-released in January 1998.
[b]When discarding residues 5 and 6. With residues 5 and 6 included, the alignment values increase to 0.88 Å, 1.28 Å and 1.09 Å.
[c]Low-temperature K intermediates of wild type, based on entry 1QHJ.
[d]Molecule A (ground state) of deposited file without publication.
[e]Molecule B (M state) of deposited file without publication.
[f]Best of the three molecules in the asymmetric unit.
[g]M: intermediate of D96N mutant.

tallography, but they also suggests that there is an open field for improving sample preparation, data collection and image processing.

4. AFM

AFM was developed 15 years ago by Binnig and coworkers [3], and brought to biology by the Hansma group, which demonstrated the feasibility of raster-scanning samples submerged in buffer solution [4]. The latter technique provides two essential advantages. First, biological samples can be studied in their native environment, a physiological buffer solution, and second, capillary forces that press the stylus onto the sample when scanning in air can be eliminated [31]. This is indeed a major prerequisite to achieve molecular resolution images of soft and fragile biological sample surfaces. Subsequent developments opened the door for imaging in air by allowing rapid oscillation of the cantilever and measuring the damping when the stylus touches the sample. Such tapping prevents capillary forces and minimizes friction, thereby allowing small molecules to be imaged, even though they are weakly adsorbed to the substrate [32,33].

Nevertheless, the highest resolution has been achieved on reconstituted membrane protein surfaces operating the microscope in the constant-force mode. The reasons are simple. First, membrane proteins are firmly packed in the bilayer and the entire assembly is immobilized on mica by van der Waals forces. Second, van der Waals forces pulling the stylus towards the sample can be balanced by electrostatic repulsions, which are adjusted by changing the ionic strength of the buffer [34]. Third, membrane proteins do not protrude more than a few nanometers from the bilayer surface, thus exposing a topography that can be contoured by a small but sharp asperity of the tip. Such contours, acquired line by line at a rate of typically 5–6 lines/s are assembled to images of superb clarity as illustrated by the topograph of LH2 complexes (Fig. 5). In this image, individual randomly arranged circular complexes reveal nine distinct protrusions exhibiting a diameter of approximately 10 Å, which protrude from the membrane by 14 Å [35]. An even higher resolution is demonstrated by the topograph of the extracellular surface of purple membrane (Fig. 6a). As documented by the diffraction pattern (Fig. 6b), a lateral resolution of 4.1 Å is feasible (diffraction order 6.9 of a trigonal lattice with unit cell dimensions $a = b = 62$ Å; $\gamma = 60°$). The average of topographs from individual trimers reveals a wealth of details. Considering the small corrugation (5 Å valley to peak), the question arises whether the accuracy of the height measurement suffices to resolve such fine details. To assess this, we have introduced the simple method to calculate not only the average, but for each pixel in this map also the S.D. [36]. S.D. maps do not only show that the reproducibility of height measurements can be significantly better than 1 Å, but S.D. maps also highlight the flexible regions of a molecule [37]. Fig. 6d shows that even the robust extracellular BR surface exhibits distinctly different regions with apparently different flexibility, yielding S.D. values ranging from 0.7 Å (on the bilayer) to 1.7 Å (on the protein). If the major sources of noise were thermal height fluctuations of the stylus, optical noise and/or electronic noise, we would not detect an interpretable signal in the S.D. map. Thus, the S.D. map reflects variability among individual BR trimers. As documented by Fig. 6a, topographs acquired under optimum recording conditions are not degraded by noise of the instrument. Hence, the question as to how height differences arise must be answered. The topography of BR as well as other membrane proteins is determined by hydrophilic polypeptide loops that connect transmembrane helices and protrude from the membranes. Such loops exhibit a certain flexibility mostly in the plane of the membrane rather than perpendicular to it. Height variations, therefore, are likely the result of lateral motion. This can conveniently be assessed by searching the position of local peaks within the lateral resolution of the topograph [38]. The result of such a search over many hundreds of unit cells is a map that gives the probability to find a peak, related (e.g.) to a loop within a resolution element. Loops with significant lateral flexibilities will have a broad position probability distribution, whereas stiff loops will be indicated by sharp peaks in the probability map. This is indicated in Fig. 6e, which shows that one major protrusion resulting from the β-turn of the loop connecting helices B and C is stiff and does not move significantly beyond the lateral resolution (4.1 Å in this case). The other protrusion is loop FG and is equally well localized, compatible with small variations among different BR structures.

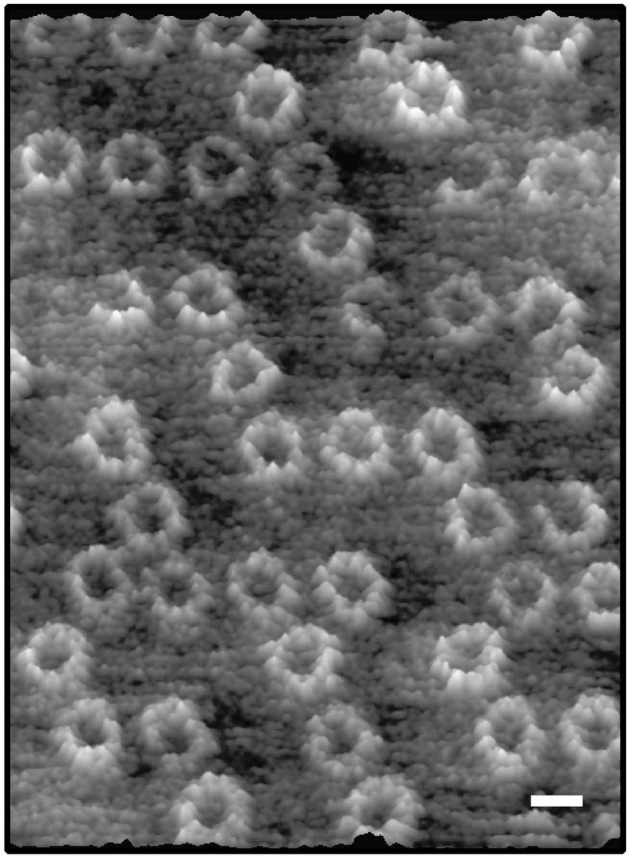

Fig. 5. LH2 of *Rubrivivax gleatinosum* are comprised of 9 α/β-heterodimers. The topograph recorded with an AFM in buffer solution under optimum conditions reveals rings that show 9 distinct protrusions that have a height of 14 Å. The scale bar is 50 Å.

The loop position probability and the potential well $E(x,y)$, in which the particular loop is trapped, are related by the Boltzmann equation

$$p(x,y) = C \exp\{-E(x,y)/kT\} \quad (1)$$

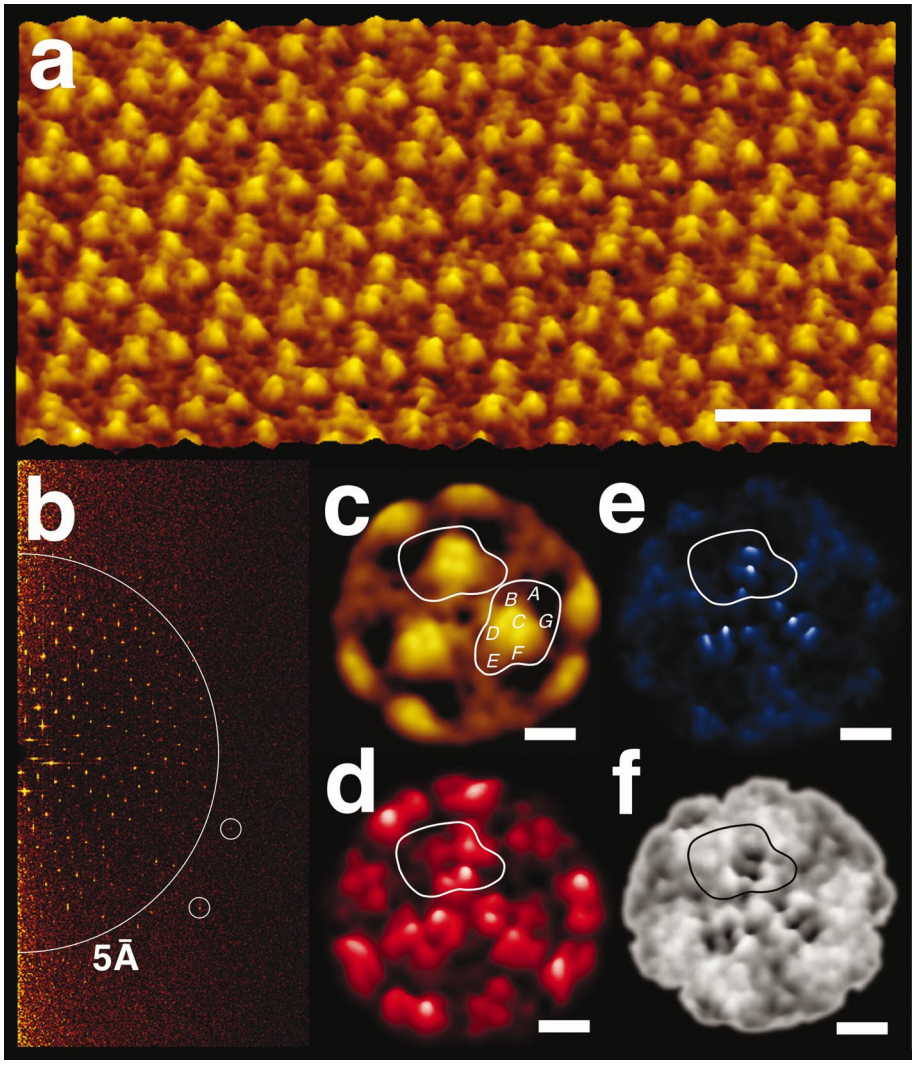

Fig. 6. High resolution topography and flexibility mapping of the extracellular surface of BR with the AFM. a: AFM topograph of the extracellular surface of BR recorded in buffer solution (10 mM Tris–HCl, pH 7.5, 150 mM KCl) (scale bar: 100 Å; full gray scale: 5 Å). b: Calculated power spectrum from raw data image (a). Half circle indicates a resolution of 5 Å, small full circles surround diffraction spots at a resolution beyond 5 Å. c: Average of 1024 topographs (scale bar: 20 Å; full gray scale: 5 Å). d: S.D. map calculated from averaging 1024 particles (scale bar: 20 Å; S.D. range: 0.7–1.7 Å). e: Position probability map acquired from 1024 aligned topographs (see also Scheuring et al. [38]) (scale bar: 20 Å; probability range 3.2*E*-4−6.4*E*-2). f: Surface energy landscape calculated from the position probability map by Eq. 2 (scale bar: 20 Å; full gray scale corresponds to 5.3 kT).

Therefore, the probability map gives an estimate of the local surface energy landscape

$$E(x,y) = -kT\ln\{p(x,y)\} - kT\ln(C) \quad (2)$$

Although this simple assessment holds only for individual loops and should be done for each loop separately, Fig. 6f has simply been calculated from Fig. 6e by applying Eq. 2. Fig. 6f displays the energy landscape of the extracellular BR surface to a good approximation, yielding a potential well for the β-turn of 5.3 kT depth. Energy landscapes have recently been calculated for a number of membrane proteins, whose loop conformations have been analyzed as described here [38].

5. Conclusions and perspectives

In membrane structure biology, the first major intermediate goal is the production and purification of mg quantities of a stable and native membrane protein. This can be studied by nuclear magnetic resonance in its solubilized form (Fernández et al., this issue, [40]) it can be crystallized in the solubilized form into 3D crystals, or it can be assembled into 2D crystals by reconstitution into the lipid bilayer. Each method has its own advantages, and hence the structural data obtained are complementary. All methods should therefore be exploited in parallel to achieve the best structural description of the protein in order to understand its function to the fullest extent.

2D crystals and their analysis by electron crystallography and AFM has a great potential, mainly because the membrane protein is reconstituted in its native environment, the lipid bilayer. Electron crystallography provides information of the 3D structure at a resolution of 3–4 Å, while AFM gives detailed information about the surface structure and dynamics of the membrane protein assessed. In all cases, the sample preparation method is critical – even the best crystals would yield unsatisfactory data if adsorbed to unsuitable substrates.

While data acquisition and processing methods for electron microscopy are now available, future developments should aim for automated data acquisition and high-speed data analyses that ultimately match those of X-ray crystallography. Concerning AFM, we note a significant progress in rapid scanning, and in increasing the sensitivity of force measurements. Furthermore, multifunctional tips are now developed that will allow the simultaneous acquisition of different signals, such as height information and electric currents. Such developments will ultimately allow the biomolecules to be observed at work.

Acknowledgements: We thank H. Lücke for Table 1 and D.J. Müller for fruitful discussions on the AFM technique. This work was supported by the Swiss National Foundation for Scientific Research (Grant 4036-44062 to A.E.), by the BIOTECH program of the EU (Grant No. BIO4-CT98-0024) and the Maurice E. Müller Foundation of Switzerland.

References

[1] Ringler, P., Heymann, B.J. and Engel, A. (2000) in: Membrane Transport (Baldwin, S.A., Ed.), pp. 229–268, Oxford University Press, Oxford.
[2] Walz, T., Smith, B.L., Zeidel, M.L., Engel, A. and Agre, P. (1994) J. Biol. Chem. 269, 1583–1586.
[3] Binnig, G., Quate, C.F. and Gerber, C. (1986) Phys. Rev. Lett. 56, 930–933.
[4] Drake, B. et al. (1989) Science 243, 1586–1589.
[5] Jap, B.K., Zulauf, M., Scheybani, T., Hefti, A., Baumeister, W., Aebi, U. and Engel, A. (1992) Ultramicroscopy 46, 45–84.
[6] Rigaud, J.-L., Mosser, G., Lacapere, J.-J., Olofsson, A., Levy, D. and Ranck, J.-L. (1997) J. Struct. Biol. 118, 226–235.
[7] Dolder, M., Engel, A. and Zulauf, M. (1996) FEBS Lett. 382, 203–208.
[8] Egelhaaf, S.U. and Schurtenberger, P. (1994) J. Phys. Chem. 98, 8560–8573.
[9] Walter, A., Vinson, P., Kaplun, A. and Talmon, Y. (1991) Biophys. J. 60, 1315–1325.
[10] Zhuang, J., Prive, G.G., Werner, G.E., Ringler, P., Kaback, R.H. and Engel, A. (1999) J. Struct. Biol. 125, 63–75.
[11] Henderson, R., Baldwin, J.M., Ceska, T.A., Zemlin, F., Beckmann, E. and Downing, K.H. (1990) J. Mol. Biol. 213, 899–929.
[12] Mitsuoka, K., Hirai, T., Murata, K., Miyazawa, A., Kidera, A., Kimura, Y. and Fujiyoshi, Y. (1999) J. Mol. Biol. 286, 861–882.
[13] Kühlbrandt, W., Wang, D.N. and Fujiyoshi, Y. (1994) Nature 367, 614–621.
[14] Murata, K., Mitsuoka, K., Hirai, T., Walz, T., Agre, P., Heymann, J.B., Engel, A. and Fujiyoshi, Y. (2000) Nature 407, 599–605.
[15] Ren, G., Cheng, A., Reddy, V., Melnyk, P. and Mitra, A.K. (2000) J. Mol. Biol. 301, 369–687.
[16] Nogales, E., Wolf, S.G. and Downing, K.H. (1998) Nature 391, 199–203.
[17] Auer, M., Scarborough, G.A. and Kühlbrandt, W. (1998) Nature 392, 840–843.
[18] Krebs, A., Villa, C., Edwards, P.C. and Schertler, G.F. (1998) J. Mol. Biol. 282, 991–1003.
[19] Li, H., Lee, S. and Jap, B.K. (1997) Nat. Struct. Biol. 4, 263–265.
[20] Rhee, K.H., Morris, E.P., Barber, J. and Kühlbrandt, W. (1998) Nature 396, 283–286.
[21] Unger, V.M., Kumar, N.M., Gilula, N.B. and Yeager, M. (1999) Science 283, 1176–1180.
[22] Williams, K.A. (2000) Nature 403, 112–115.
[23] Fujiyoshi, Y., Mizusaki, T., Morikawa, K., Yamagishi, H., Aoki, Y., Kihara, H. and Harada, Y. (1991) Ultarmicroscopy 38, 241–251.
[24] Downing, K.H. (1991) Science 251, 53–59.
[25] Fujiyoshi, Y. (1998) Adv. Biophys. 35, 25–80.
[26] Vonck, J. (2000) Ultramicroscopy 85, 123–129.
[27] Crowther, R.A., Henderson, R. and Smith, J.M. (1996) J. Struct. Biol. 116, 9–16.
[28] Luecke, H. (2000) Biochim. Biophys. Acta 1460, 133–156.
[29] Heymann, J.B., Müller, J.D., Landau, E.M., Rosenbusch, J.P., Pebay-Peyroula, E., Büldt, G. and Engel, A. (1999) J. Struct. Biol. 128, 243–249.
[30] Stahlberg, H., Braun, T., de Groot, B., Philippsen, A., Borgnia, M.J., Agre, P., Kühlbrandt, W. and Engel, A. (2000) J. Struct. Biol. 132, 133–141.
[31] Weisenhorn, A.L., Hansma, P.K., Albrecht, T.R. and Quate, C.F. (1989) Appl. Phys. Lett. 54, 2651–2653.
[32] Hansma, P.K. et al. (1994) Appl. Phys. Lett. 64, 1738–1740.
[33] Putman, C.A.J., Vanderwerf, K.O., de Grooth, B.G., Vanhulst, N.F. and Greve, J. (1994) Appl. Phys. Lett. 64, 2454–2456.
[34] Müller, D.J., Fotiadis, D., Scheuring, S., Müller, S.A. and Engel, A. (1999) Biophys. J. 76, 1101–1111.
[35] Scheuring, S., Reiss-Husson, F., Engel, A., Rigaud, J.L. and Ranck, J.L. (2001) EMBO J. 20, 3029–3035.
[36] Schabert, F.A. and Engel, A. (1994) Biophys. J. 67, 2394–2403.
[37] Müller, D.J., Fotiadis, D. and Engel, A. (1998) FEBS Lett. 430, 105–111.
[38] Scheuring, S., Müller, D.J., Stahlberg, H., Engel, H.-A. and Engel, A. (2001) Eur. Biophys. J., in press.
[39] Pebay-Peyroula, E., Rummel, G., Rosenbusch, J.P. and Landau, E.M. (1997) Science 277, 1676–1681.
[40] Fernández, C., Hilty, C., Bonjour, S., Adeishvili, K., Pervushin, K. and Wüthrich, K. (2001) FEBS Lett. 504, 173–178.
[41] Hunte, C. (2001) FEBS Lett. 504, 126–132.
[42] Nollert, P., Qiu, H., Caffrey, M., Rosenbusch, J.P. and Landau, E.M. (2001) FEBS Lett. 504, 179–186.
[43] Levy, D., Chami, M. and Rigaud, J.-L. (2001) FEBS Lett. 504, 187–193.
[44] de Groot, B.L., Engel, A. and Grubmüller, H. (2001) FEBS Lett. 504, 206–211.